VISION-BASED CONTROL OF FIXED-WING UNMANNED AERIAL VEHICLE FOR AUTONOMOUS ROAD-FOLLOWING

João Paulo de Souza, jpsouza@ita.br
Elder Moreira Hemerly, hemerly@ita.br
Instituto Tecnológico de Aeronáutica, ITA – Pça. Mal. Eduardo Gomes, 50 – Vila das Acácias – São José dos Campos - SP

Abstract. *Navigation and control techniques using the GPS signals have problems in areas where the terrain or other obstacles can jam or block the satellite signal. Navigation systems based on vision emit no external signs, are passive and low cost. This work aims to enable the autonomous navigation of a fixed-wing unmanned aerial vehicle (UAV) for road tracking using only image processing and inertial sensors. Image processing algorithms were implemented to generate waypoints and projection of the image reference frame to the world reference frame, thereby enabling the design of strategies for lateral and altitude control. Performance evaluation is carried out with a realistic UAV model and virtual scenario using the FlightGear Simulator. This simulator provides visualization of three-dimensional models, which run in accordance with the information of position and attitude received from the control algorithms implemented in MatLab.*

Keywords*: Vision, UAV, Tracking Trajectory, Navigation, Image Processing*

1. INTRODUCTION

Unmanned aerial vehicles (UAV's) are remotely piloted or autonomous aircraft that can carry cameras, sensors, communication equipments, among others. The UAV's have very important in applications that include traffic and environmental monitoring, pest control and fire, search and rescue, border patrol, aerial surveillance, crop and flock inspection, police surveillance of urban areas, inspection of power transmission lines and oil products, assistance in disaster and military applications.

The versatility and low cost of UAV's are the main factors for the increase in its use both in public and in private sectors. Some of the disadvantages of the UAV's include payload capacity, and limited supply of energy. However, there are several advantages associated with the use of UAV's that override these limitations. Because they are more maneuverable and are not operated by pilot, their missions are in general more complex, such as very low altitude flights or flying through hostile environment. The main advantage of UAV is the operational cost, which is up to three times cheaper than a traditional aircraft. Besides having a lower cost than manned aircraft, they are more easily transported and can be launched even on uneven terrain.

Standard techniques that rely heavily on GPS for navigation and control will have difficulties in urban environments or hostile environments in which the satellite signals can be easily blocked, jammed or have their accuracy degraded. The computer vision is an important sensor for UAV's operating in natural environments. A sequence of video images contains a large amount of information that can be used for navigation and control, detection and identification of objects, obstacle avoidance and many other tasks. Unlike systems based on radar or laser, the computer vision is passive and emits no external signals. As a result, systems based on vision can be small in size, reducing the load of the UAV platform.

The contribution of this work is the development of image processing and attitude and position control for easy implementation, aiming at UAV applications. A comparison of performance between two techniques for lateral control is realized, keeping the parameters of the autopilot unaltered. The discussion focuses on the characteristics and capabilities of the control based on vision for civil and military use. The main difference with respect to Niculescu (2001) and Frew (2004) are: a) Niculescu (2001) consider only lateral control, without addressing the image processing task; b) no performance comparison between the 2 strategies is carried out in Frew (2004), and c) neither employs *FlightGear* for visualization, which is efficient and freely available.

2. UAV MODEL

The general equations of motion presented in this section were developed for a rigid aircraft and are divided into three sets: force equations, moment equations and kinematics equations (Roskan, 2001).

$$\begin{aligned} m\left(\dot{U} - VR + WQ\right) &= -mg\sin\left(\Theta\right) + F_{A_x} + F_{T_x} \\ m\left(\dot{V} + UR - WP\right) &= mg\sin\left(\Phi\right)\cos\left(\Theta\right) + F_{A_y} + F_{T_y} \\ m\left(\dot{W} - UQ + VP\right) &= mg\cos\left(\Phi\right)\cos\left(\Theta\right) + F_{A_Z} + F_{T_Z} \end{aligned} \tag{1}$$

$$\begin{aligned}
&I_{xx}\dot{P} - I_{xz}\dot{R} - I_{xz}PQ + \left(I_{zz} - I_{yy}\right)RQ = L_A + L_T \\
&I_{xx}\dot{Q} + \left(I_{xx} - I_{zz}\right)PR + I_{xz}\left(P^2 - R^2\right) = M_A + M_T \\
&I_{zz}\dot{R} - I_{xz}\dot{P} + \left(I_{yy} - I_{xx}\right)PQ + I_{xz}QR = N_A + N_T
\end{aligned} \tag{2}$$

$$\begin{aligned}
&P = \dot{\Phi} - \dot{\Psi}\sin(\Theta) \\
&Q = \dot{\Theta}\cos(\Phi) + \dot{\Psi}\cos(\Theta)\sin(\Phi) \\
&R = \dot{\Psi}\cos(\Theta)\cos(\Phi) - \dot{\Theta}\sin(\Phi)
\end{aligned} \tag{3}$$

Where m is the mass of the UAV; U, V, W are the UAV linear velocities components about XYZ; P, Q, R are the UAV angular velocities components about XYZ; g is the acceleration of gravity; Φ, Θ, Ψ are the Euler angles of the UAV; F_{Ax}, F_{Ay}, F_{Az} are the aerodynamic force components along XYZ; F_{Tx}, F_{Ty}, F_{Tz} are the thrust force components along XYZ; I_{xx}, I_{yy}, I_{zz} are the UAV moments of inertia about XYZ; I_{xy}, I_{yz}, I_{xz} are the UAV products of inertia about XYZ; L_A, M_A, N_A are the aerodynamic moment components about XYZ; L_T, M_T, N_T are the thrust moment components about XYZ.

The Equations (1)-(3) are necessary for the understanding and use of mathematical model for the aerodynamic forces and moments that act on the UAV. These describe the aerodynamic behavior of an UAV, which were used in the analysis and design of the control system.

In this work we used the typical model of the UAV and autopilot design presented and developed in Hemerly et al. (2006). Figure 1 shows the block diagram of the autopilot.

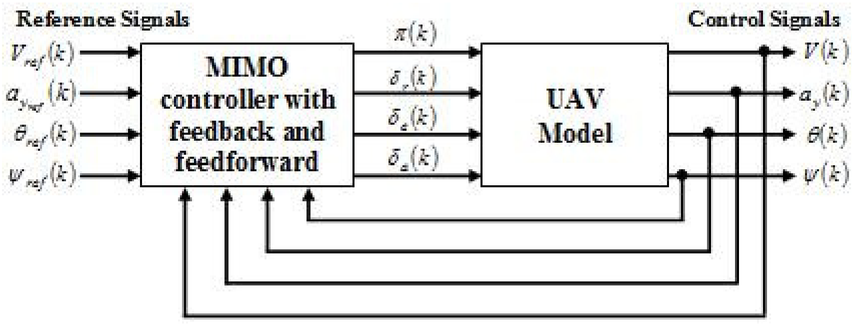

Figure 1. Autopilot block diagram.

In Figure 1, V and V_{ref} are the measured and reference linear velocity, respectively; a_y and a_{yref} are the measured and reference lateral acceleration, respectively; θ and θ_{ref} are the measured and reference pitch angle, respectively; ψ and ψ_{ref} are the measured and reference yaw angle, respectively; π, δ_r, δ_e and δ_a are the throttle, rudder, elevator and aileron commands.

In section 5, simulation results for a realistic UAV model using the control techniques implemented in this work are presented and discussion.

3. COMPUTER VISION

There are many applications of computer vision techniques. Traditionally, most of the computer vision systems have been designed for industrial and military applications. Common military applications include target recognition, visual guidance for autonomous vehicles, recognition and interpretation of images. Common industrial applications include visual inspection of parts and automated control systems.

In this work, the interaction with the user is only required to classify the pixels as positive (track) or negative (non-track) for a particular training sample (Figures 2a and 2b). The statistics for a sampled region is computed through the mean and standard deviations of the interest pixels.

We use a connected components analysis algorithm (Fig. 2c) available in the image processing toolbox of the *MatLab*, which is a method of identifying objects, regions and features to convert the previous segmentation in adjacent regions. This algorithm marks regions with areas smaller than a give threshold (window). This window is placed on each pixel of the background, and the algorithm assigns it to the class that is the closest to its neighborhood. In this work were selected windows with up to 4 pixels square area.

Finally, using the location information of regions selected by the user in classification step, we determine the class to be defined as the track (Fig. 2d).

A disadvantage of these techniques is that only the local information is used. One way to enter the global information is through models. The techniques of the Hough transform (Fig. 2e) are well known techniques of this type that can be applied to straight lines, circles and any other kind of curves that can be expressed by a small set of parameters. In this work, we consider only the problem of detecting straight lines in images with the application of Hough transform.

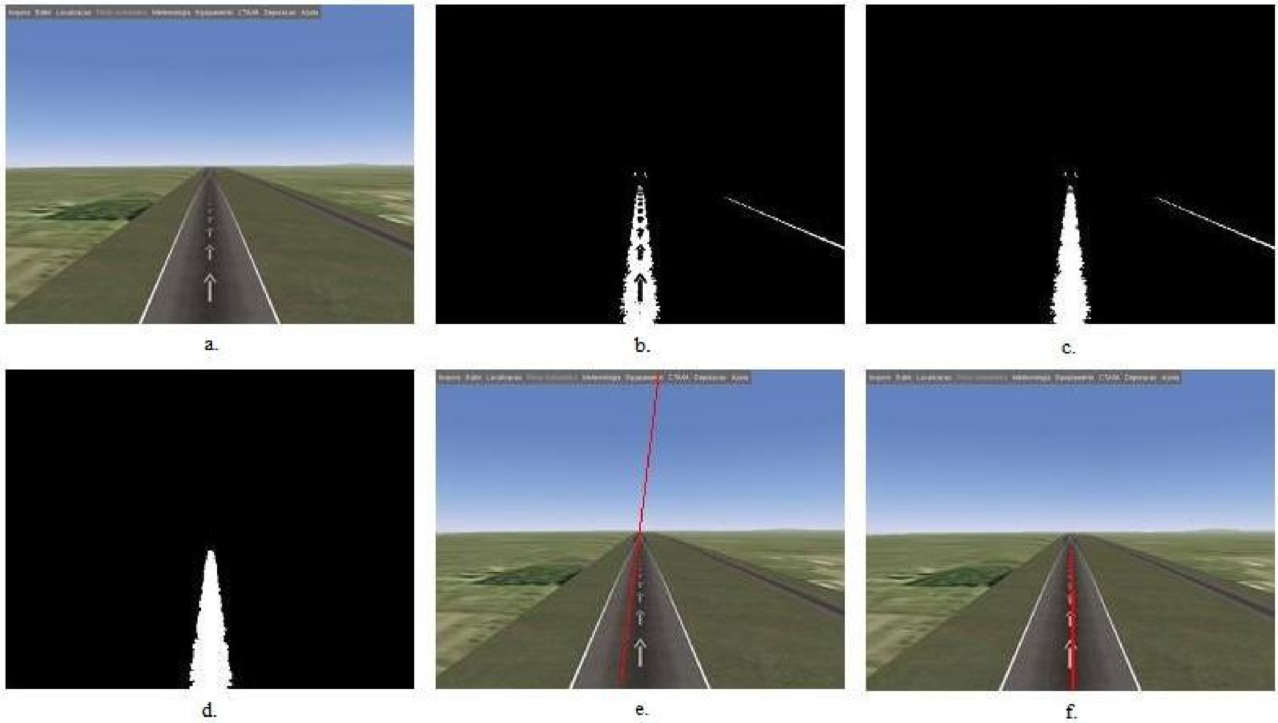

Figure 2. Road detection algorithm. a) Original Image. b) Pixels Classification. c) Connected components analysis. d) Holes removal. e) Hough transform. f) Robust line fitting.

Representation in polar coordinates of a straight line is used in processing, to avoid infinitely large slope coefficients for straight lines parallel to y-axis.

A robust alignment (Fig. 2f) of the line using the least squares method (LSM) is applied to analyze the position and orientation of the center of the runway. The data points used as input for the algorithm that implements the LSM are obtained from an algorithm for detecting edges. These edges are taken as the edges of the track, which after being subjected to LSM return the center of the runway.

4. NAVIGATION AND CONTROL

4.1. Projection equations

The set of points in the image that represents the centerline of the track are the waypoints to be flown by UAV. The waypoints are defined, in general, by latitude, longitude, altitude, direction, aircraft speed or speed relative to the ground, flying time, among others. However, until the moment, waypoints are points (pixels) defined in the reference plane of the image (X_i, Y_i). The Figure 3 shows the layout of the camera relative to the UAV and image reference system as seen by the camera.

As can be seen in Figure 3, the center of rotation of the *gimbal* (C) at which the camera is fixed is not on the center of gravity (A) of UAV. The same as sensing element of the camera is not in the center of rotation of the *gimbal*.

To obtain the equations of projection is necessary first to apply the model of the pinhole camera, and then align the coordinate systems by means of rotations and translation.

In the pinhole camera model, the location of a point in the coordinate system of the camera (X_C, Y_C, Z_C) is related to a point in the image by the equation:

$$x_i = f \cdot \frac{x_c}{z_c}, \; y_i = f \cdot \frac{y_c}{z_c} \tag{4}$$

where f is the focal length of the camera in pixel dimension; x_c, y_c, z_c are the coordinates of a point in the coordinate system of the camera; x_i, y_i are the coordinates of a point in the coordinate system of the image; $X_AY_AZ_A$ is the coordinate system of the UAV; and $X_WY_WZ_W$ is the coordinate system of the world.

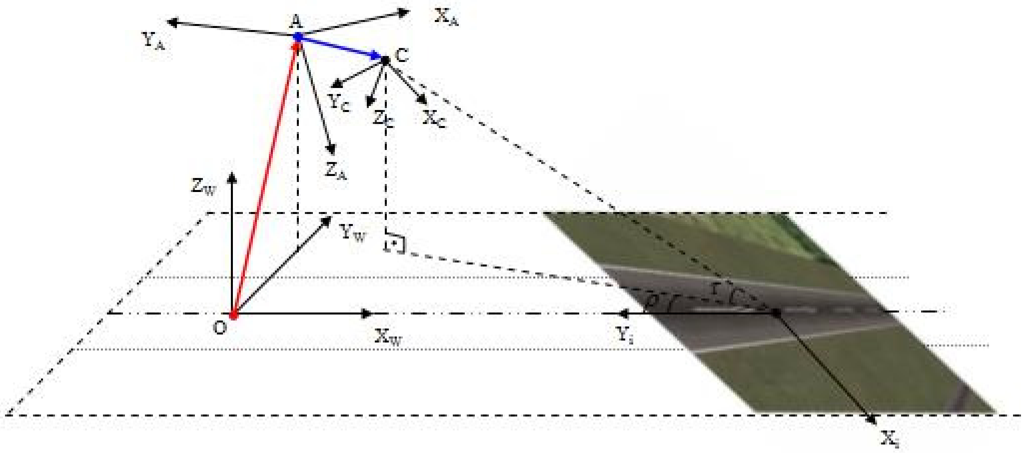

Figure 3. Coordinate systems of image, camera, aircraft and runway.

Equation (5) shows the matrices of rotation (**R**$\mathbf{R_x}$, $\mathbf{R_y}$, $\mathbf{R_z}$) around the axis x, y and z, respectively, counter-clockwise:

$$\mathbf{R_x}(\alpha)=\begin{bmatrix}1 & 0 & 0\\ 0 & \cos(\alpha) & -\sin(\alpha)\\ 0 & \sin(\alpha) & \cos(\alpha)\end{bmatrix},\ \mathbf{R_y}(\beta)=\begin{bmatrix}\cos(\beta) & 0 & \sin(\beta)\\ 0 & 1 & 0\\ -\sin(\beta) & 0 & \cos(\beta)\end{bmatrix},\ \mathbf{R_z}(\gamma)=\begin{bmatrix}\cos(\gamma) & -\sin(\gamma) & 0\\ \sin(\gamma) & \cos(\gamma) & 0\\ 0 & 0 & 1\end{bmatrix} \tag{5}$$

Finally, the translation matrix is defined by:

$$\mathbf{T}=\begin{bmatrix}t_x\\ t_y\\ t_z\end{bmatrix} \tag{6}$$

where t_x, t_y, t_z is the components of the translation matrix.

For the alignment of the camera two rotations are required and one translation as in Eq. (7). This is because the camera has only movements of pan and tilt.

$$\begin{bmatrix}x_c\\ y_c\\ z_c\end{bmatrix}=\mathbf{R_y}(\tau)\cdot\mathbf{R_z}(\rho)\cdot\begin{bmatrix}x_A\\ y_A\\ z_A\end{bmatrix}+\mathbf{T} \tag{7}$$

According to Fig. 3, this alignment requires first a rotation of angle τ (tilt angle of the camera) around the axis Y_C in counter-clockwise and a second rotation, of angle ρ (pan angle of the camera) around the axis Z_C in counter-clockwise, as in Eq. (7).

4.2. Arctan controller

This nonlinear lateral control strategy developed in Frew (2004) supposes that the speed of the aircraft is constant. The goal is to bring the aircraft from point Wp_1 to point Wp_2 located on the runway, as shown in Fig. 4.

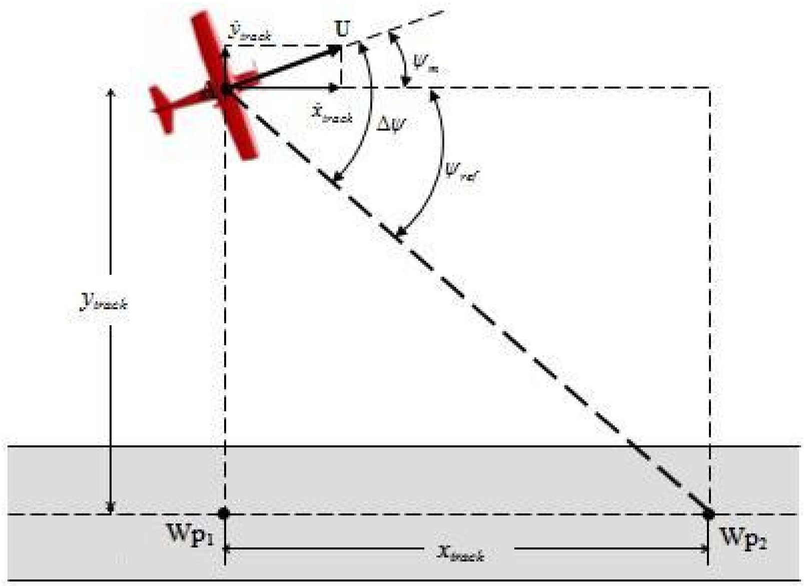

Figure 4. Arctan Controller.

Given the aircraft's current position (Wp$_1$) and the next waypoint (Wp$_2$), the heading reference ψ_{ref} can be calculated from equation:

$$\psi_{ref} = \arctan(-y_{track}, x_{track}) \tag{8}$$

where y_{track} and x_{track} are obtained from the geometry between the roll angle, altitude measured of aircraft and projection equations (subsection 4.1 and fig. 3).

The measured heading of the aircraft ψ_m is calculated from the components of its velocity, which obtained from the UAV model developed in section 2:

$$\psi_m = \arctan(\dot{y}_{track}, \dot{x}_{track}) \tag{9}$$

The signal error of the heading is defined by the difference between the reference and measured headings, as in Eq. (10).

$$e = \Delta\psi = \psi_m - \psi_{ref} \tag{10}$$

This signal is to be brought to zero by the proportional integral control law with the saturation limit of $\pm$ 0.2 rad/s.

4.3. Velocity ratio controller

This strategy developed in Niculescu (2001) is also a nonlinear lateral control that assumes the speed of the aircraft as being constant. As in the previous strategy, the goal is to bring the aircraft to its current position (point A) to the next waypoint (point Wp$_2$), as shown in Fig. 5.

From the geometry of similarity between the triangles ABC and ADE, this control strategy is based on the establishment of the position and speed of the vehicle according to the relationship:

$$\frac{\dot{x}_{track}}{k \cdot x_{track}} = \frac{\dot{y}_{track}}{y_{track}} \tag{11}$$

$$E = k \cdot x_{track} \cdot \dot{y}_{track} - y_{track} \cdot \dot{x}_{track} = 0 \tag{12}$$

$$\omega_{CMD} = K_R \cdot E = K_R\left(k \cdot x_{track} \cdot \dot{y}_{track} - y_{track} \cdot \dot{x}_{track}\right) \tag{13}$$

The parameter k determines the speed with which the aircraft converges to the reference trajectory and the parameter K_R is determined interactively by simulation until a good tracking trajectory is found without overshoot. For safety, it is imposed a limit of saturation of $\pm$ 0.2 rad/s in the angular speed at the reference ω_{CMD}. This variable is integrated for supply the yaw reference. The values of k = 0.000025 and K_R = 0.24 and were found satisfactory for this lateral control law.

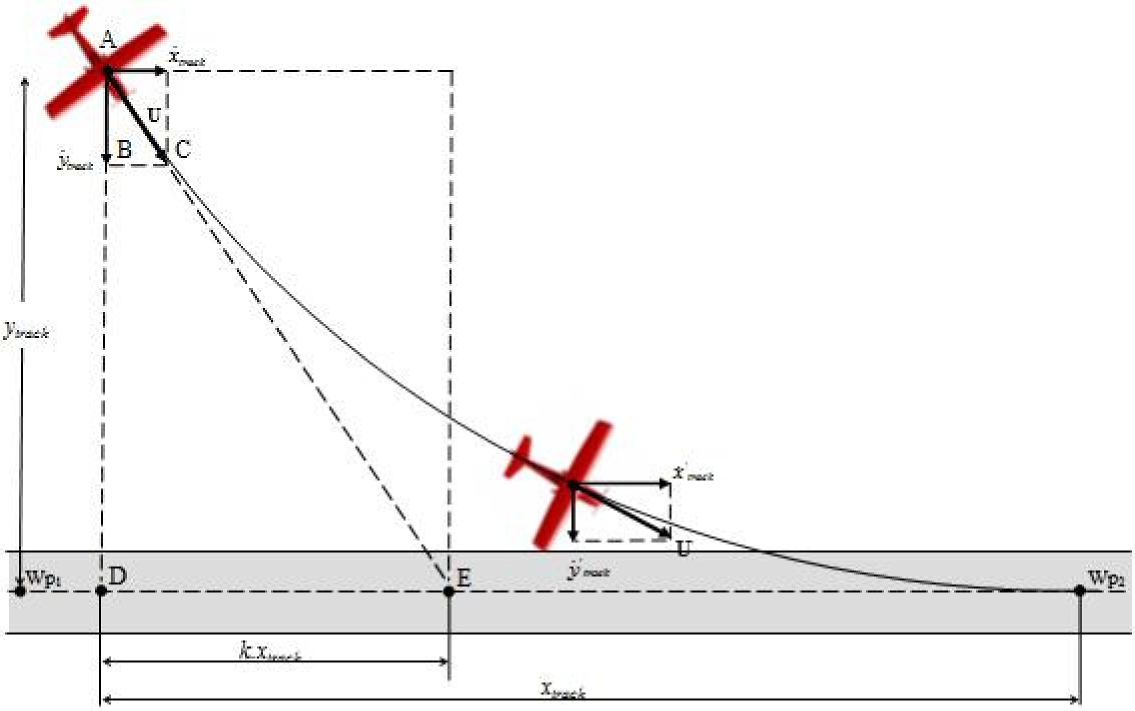

Figure 5. Velocity ratio controller.

5. RESULTS

This section presents the results of simulation for the UAV model developed in section 2 applying the laws of lateral control presented in subsections 4.2 and 4.3. The UAV first is in equilibrium condition, when the signals are then applied as reference. The variables to be controlled by the autopilot are speed, lateral acceleration, yaw angle and pitch angle (inner loop).

5.1. Arctan controller

The Figure 6 shows the signs of reference for the MIMO controller with feedback and feedforward signals and the measured output in the UAV model shown in section 2 (see Fig. 1) for a simulation horizon of 8000 steps. The UAV is in the condition of equilibrium up to 1000 steps of simulation, when the lateral and altitude controls (Fig. 7) are then applied. The reference linear velocity is 12 m/s, and lateral acceleration reference is 0 m/s^2.

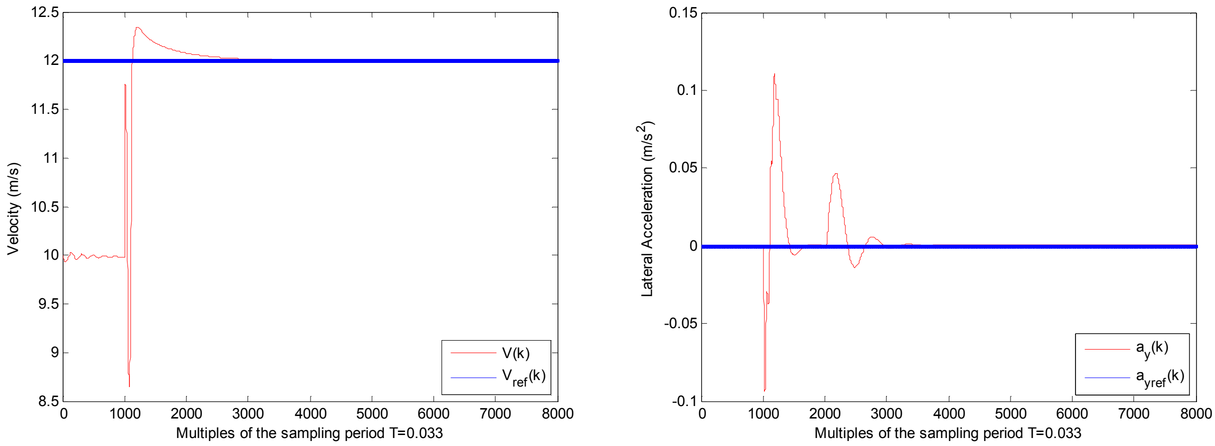

a. b.

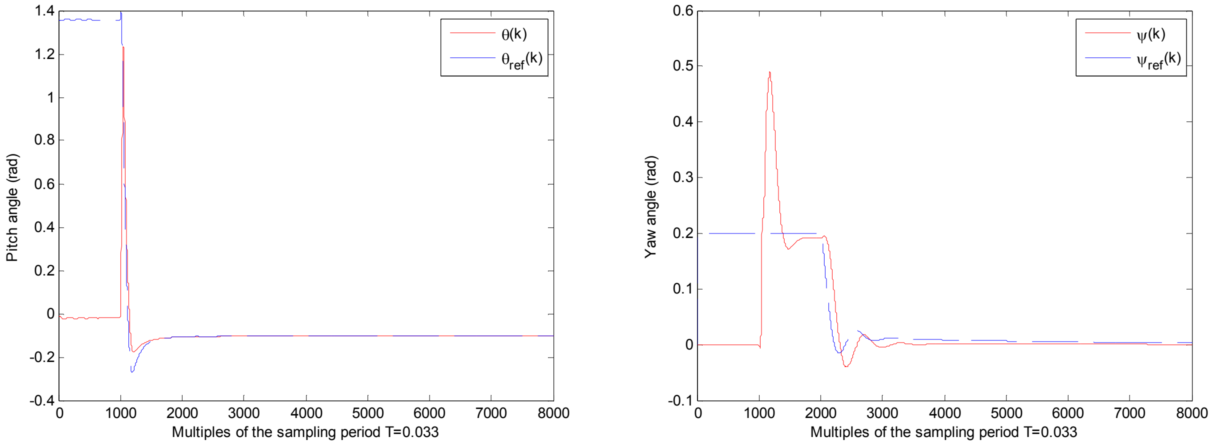

c. d.

Figure 6. Variables controlled by the autopilot and its references with the arctan controller. a) Velocity measured and reference. b) Lateral acceleration measured and reference. c) Pitch angle measured and reference. d) Roll angle measured and reference.

The reference for the pitch and yaw angles are generated by the external loop of the proportional integral (PI) guidance type (see Tab. 1). The pitch angle in equilibrium condition is about 1.36 rad. The yaw angle reference is limited to ± 0.2 rad. This explains why the reference signal keeps the value of 0.2 rad to about 2000 steps of simulation.

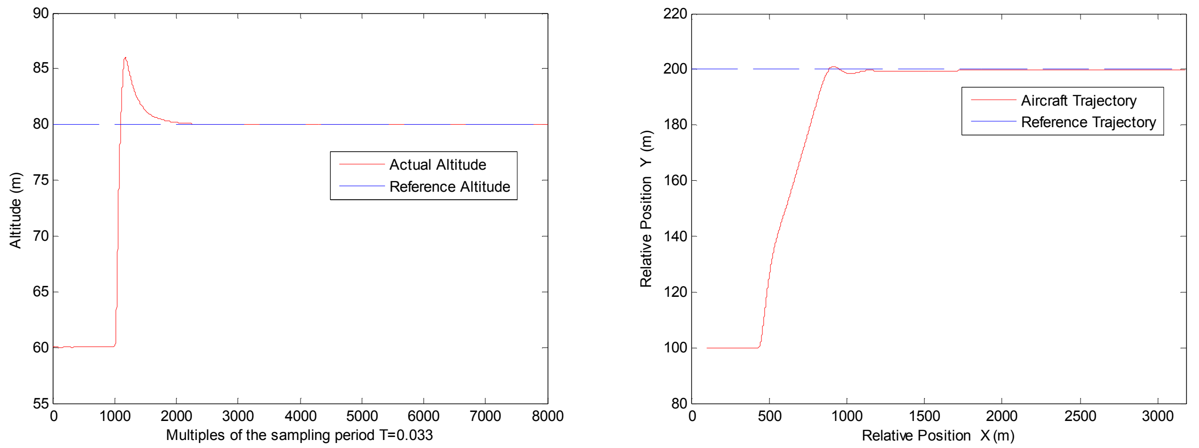

a. b.

Figure 7. Altitude and relative position of the aircraft with the arctan controller. a) Altitude measured and reference. b) Relative trajectory measured and reference.

As can be seen, the error converge to zero. We obtained a good tracking for the pitch angle, and the other variables reached the reference in less than 3000 steps of simulation after the application of control signals.

Table 1. Gains for the PI controllers with the Arctan controller.

	Linear Velocity	*Lateral Acceleration*	*Pitch Angle*	*Yaw Angle*	*Altitude Hold*
k_p	1.6	0.119	2.5	0.119	0.068
k_i	0.075	0.00009	0.8	0.001	0.0056

The control signals are defined by: throttle (π (k)) limited between the values from 0 to 1 (dimensionless value), the rudder deflection (δ_r (k)) limited to ± 1 rad, the elevator deflection (δ_e (k)) limited to ± 0.4 rad and the aileron deflection (δ_a (k)) limited to ± 1 rad. The parameters k_p and k_i are the proportional and integral gains of the PI controllers.

5.2. Velocity ratio controller

Similar to the previous section, the Fig. 8 shows the signs of reference for the MIMO controller with feedback and feedforward and measured signals in the output of the UAV model for the velocity ratio controller.

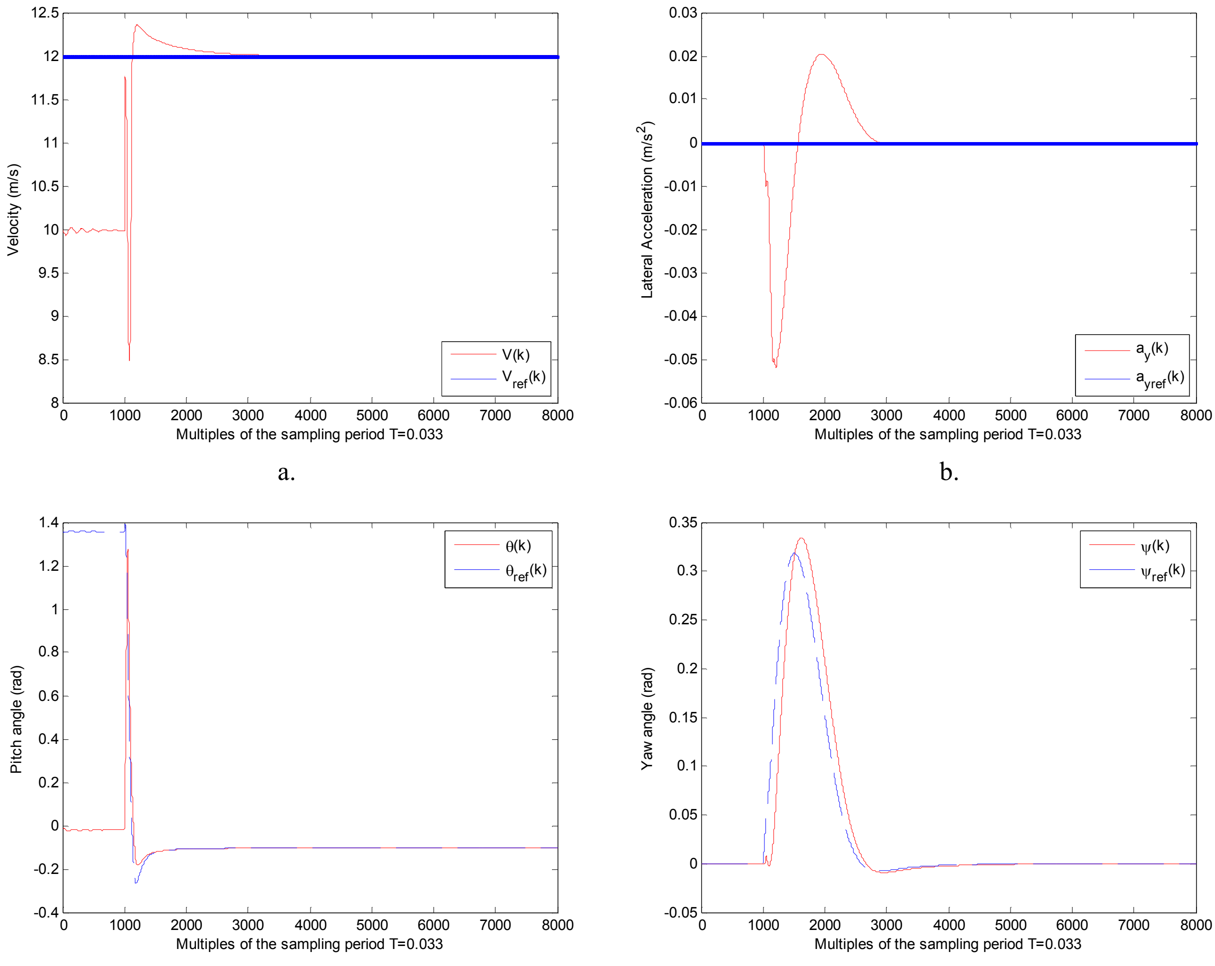

Figure 8. Variables controlled by the autopilot and its references with the velocity ratio controller. a) Velocity measured and reference. b) Lateral acceleration measured and reference. c) Pitch angle measured and reference. d) Roll angle measured and reference.

As can be seen, the error converge to zero. We obtained a good tracking for the pitch angle, and the other variables reached the reference in less than 3000 steps of simulation after the control signals application. The Figure 9 shows the altitude obtained for the pitch angle shown in the Fig. 7 and the trajectory of the aircraft due to the technique of lateral control, respectively.

Table 2. Gains for the P and PI controllers with the velocity ratio controller.

	Linear Velocity	*Lateral Acceleration*	*Pitch Angle*	*Yaw Angle*	*Altitude Hold*	*Angular Velocity*
k_p	1.6	0.119	2.5	0.119	0.068	0.000025
k_i	0.075	0.00009	0.8	0.001	0.0056	-

Different reference values were used to evaluate the performance of controllers. It is important to express the performance achieved is not optimal, so it is possible to obtain better results.

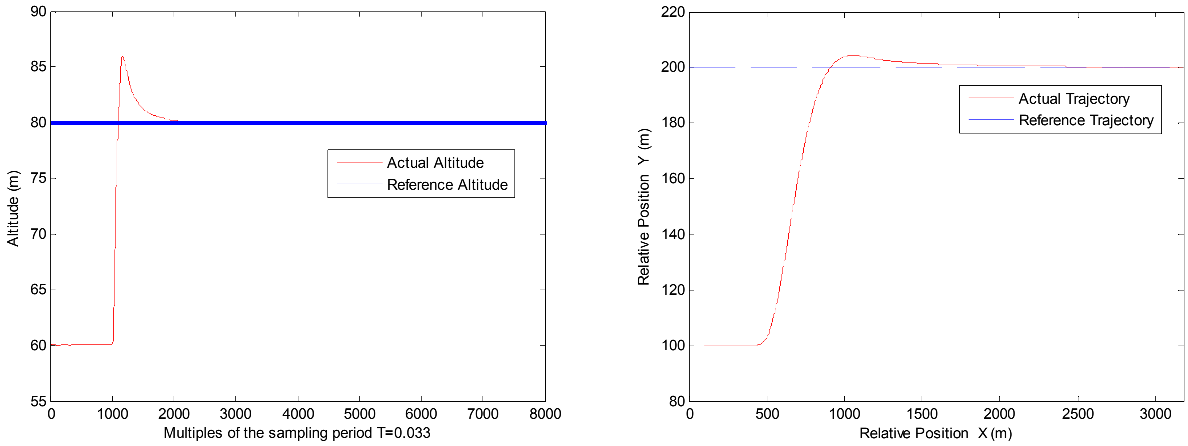

a. b.

Figure 9 Altitude and position relative of the aircraft with the velocity ratio controller. a) Altitude measured and reference. b) Relative trajectory measured and reference.

The two techniques for lateral control were implemented in *MatLab* software in 2 different ways: the package *Simulink* blocks (simple and s-functions) and the programming code on file ".m". Data of time, latitude, longitude, altitude, roll, pitch and yaw angles are sent to *FlightGear* via IP address. This simulator has the advantage of having known scenarios, with several airports available with their surroundings.

Figure 10 shows simulations results for the lateral control of the velocity ratio type. The starting point for the simulations carried out in *Simulink* was a position located on top of the entrance of the Electronics Division of Technological Institute of Aeronautics, with known latitude and longitude. The reference trajectory is given by the center of the airport runway at São José dos Campos.

Figure 10. Virtual scenario of the aircraft with the velocity ratio controller flying over São José dos Campos airport.

The algorithms were implemented by a ".m" file. Thus, a ".dll" file that captures the screen image of the simulator is called as a subroutine by *MatLab*. This dll simulates the camera taking a frame for processing by the vision algorithm.

5.3. Robustness to Image Noise

Due to image noise, the waypoints are not precisely known. The effects of this noise are evaluated by simulations. For a variance of 5 m in the waypoint positions (3D reference trajectory), the obtained altitude (Fig. 11a) and relative position (Fig. 11b), for the arctan controller, indicate no substantial difference with respect to the noiseless case.

The same applies to the altitude (Fig. 11c) and relative position (Fig. 11d), for the velocity ratio controller with noise.

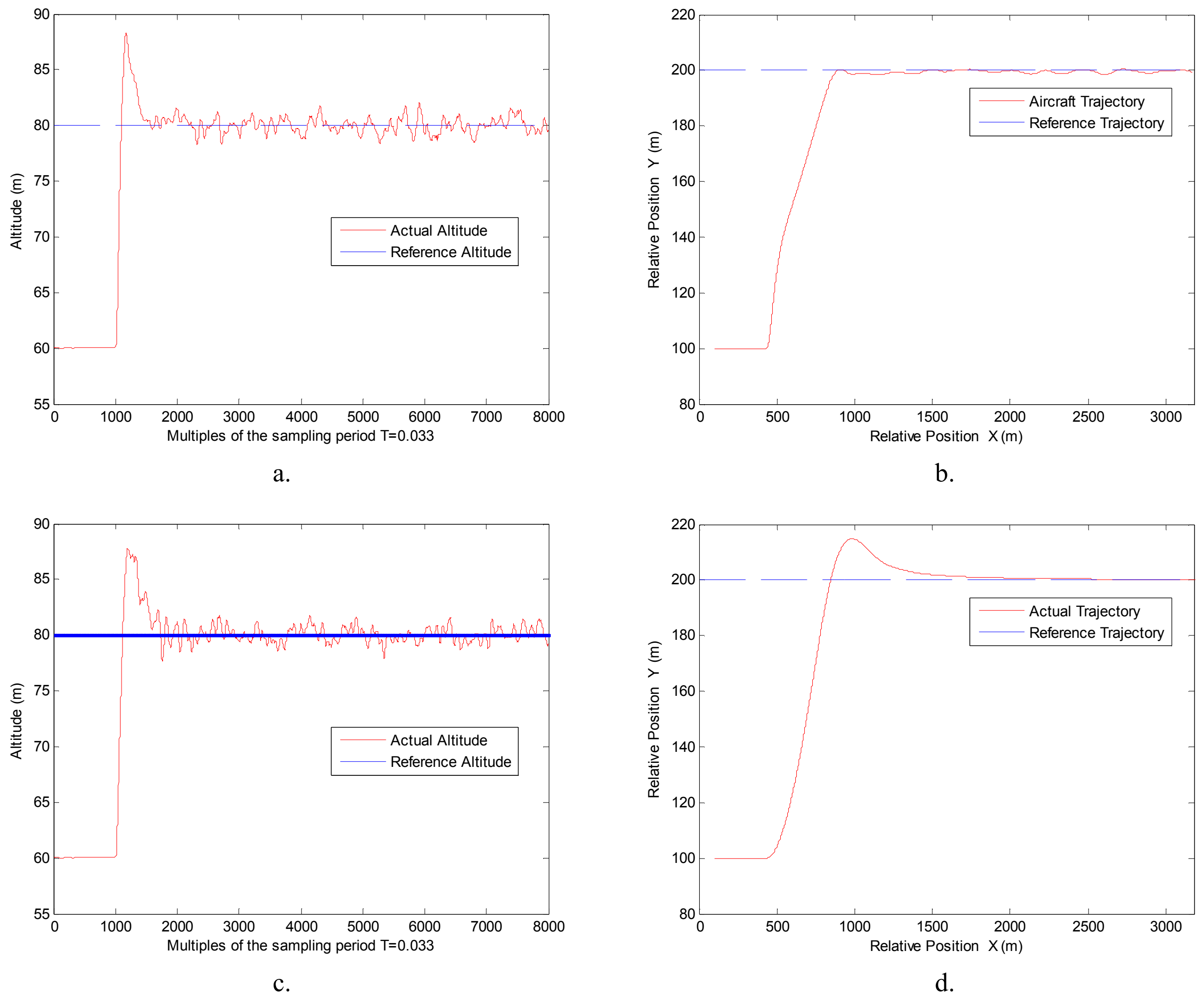

Figure 11. Altitude and relative position of the UAV with image noise. a) Altitude of the UAV with the arctan controller. b) Relative position of the UAV with the arctan controller. c) Altitude of the UAV with the velocity ratio controller. d) Relative position of the UAV with the velocity ratio controller.

6. CONCLUSIONS

Techniques of image processing for detection and localization of the center of a track were implemented,and used for comparing two techniques for lateral control existent in the literature. Therefore, a system for navigation and control of UAVs based on computational vision was presented and implemented in a virtual scenario, by employing a free software for flight visualization. The performances of the control strategies are directly related to the PI parameters of the yaw controller for the arctan controller; and to the parameters k and K_R , for the velocity ratio controller.

Future works will address applications for night vision and development of electronics onboard.

7. REFERENCES

Frew, E., Mcgee, T., Kim, Z., Xiao, X., Jackson, S., Morimoto, M., Rathinam, S., Padial, J., Sengupta, R., 2004, “Vision-Based Road-Following Using a Small Autonomous Aircraft”, IEEE Aerospace Conference.

Hemerly, E. M., Neto, N. S. B., Maciel, B. C. O., Goes, L. C. S., 2006, “Identificação e Controle de Veículos Autônomos Não Tripulados com Asa Fixa”, XVI Congresso Brasileiro de Automática, Salvador-BA, pp. 1231-1236.

Niculescu, M., 2001, “Lateral Track Control Law for Aerosonde UAV”, Proceedings of the 39TH AIAA Aerospace Sciences Meeting and Exhibit.

Roskan, J., 2001, “Airplane Flight Dynamics and Automatic Flight Controls. Part 1”, Lawrence, KS, DARcorp.

8. RESPONSIBILITY NOTICE

The author(s) is (are) the only responsible for the printed material included in this paper.